Section 9

Development of and studies with coupled ocean-atmosphere models

Numerical simulations of the intensity change of Typhoon Choiwan (2009) and the oceanic response

Akiyoshi Wada
*Meteorological Research Institute, Tsukuba, Ibaraki, 305-0052, JAPAN
awada@mri-jma.go.jp

1. Introduction

Interactions between typhoons and the ocean are known to be important for predicting their intensity changes. In addition, a strong wind curl accompanied by typhoons induces sea surface cooling by passage of a TC, and causes variations in pCO_2 in the upper ocean. The concentration of pCO_2 is a function of the concentration of hydrogen ions, which is calculated by given water temperature, salinity, dissolved inorganic carbon (DIC) and total alkalinity (ALK). Wada et al. (2011a, b) reported that a simple chemical scheme coupled with an ocean general circulation model (Wada et al., 2011a) or coupled with a nonhydrostatic atmosphere model coupled with a multilayer ocean model and the third generation ocean wave model enabled us to simulate variations in pCO_2 and air-sea CO_2 flux caused by Typhoons Tina and Winnie (1997) and Typhoon Hai-Tang (2005). However, the variations in pCO_2 could not be validated for numerical simulations of Typhoon Hai-Tang (2005) due to lack of observation.

Bond et al. (2011) reported that ΔpCO_2, the water minus air value, increased dramatically giving a maximum value of 55 μatm and then it slowly decreases at the surface mooring buoy named the Kuroshio Extension Observatory (KEO) buoy by passage of Typhoon Choiwan in 2009. In order to clarify the mechanism of the variations in pCO_2 in the upper ocean by passage of Choiwan, numerical simulations were performed using a nonhydrostatic atmosphere model coupled with the multilayer ocean model and the third generation ocean wave model.

2. Experiment design

The specification of numerical simulations performed by a nonhydrostatic atmosphere model coupled with the multilayer ocean model, the ocean wave model and the simple chemical scheme is given in this section. The computational domain is 3240 km x 3960 km with a horizontal grid spacing of 6 km. The model has 40 vertical levels with variable intervals from 40 m for the lowermost (near-surface) layer to 1180 m for the uppermost layer. The model has maximum height approaching nearly 23 km. The time step of the nonhydrostatic model is 15 s. The length of the time step of the ocean model is six times that of the atmosphere model. The initial depth of the mixed layer is determined from oceanic reanalysis data, calculated using the MRI ocean variational estimation (MOVE) system (Usui et al., 2006), by assuming a difference in the value of density from the surface of no more than 0.25 kg m^{-3} and the depth of the mixed layer is limited to 200 m. The base of the thermocline is limited to 600 m and water depth is limited to 2000 m.

Table 1 shows a list of numerical experiments. Acronyms are the same as Wada (2012), which is determined from the model whether noncoupled atmosphere or coupled atmosphere-ocean model, their horizontal resolution, the type of atmospheric initial and lateral boundary condition ("G" means global analysis data made in Japan Meteorological Agency), horizontal resolution of oceanic reanalysis data, and cloud physics ("I" means inclusion of ice phase).

Table 1 A list of numerical simulations

	Coupled ocean / Noncoupled	Horizontal resolution of oceanic reanalysis data
A6G5I	Noncoupled	0.5
A6G1I	Noncoupled	0.1
C6G5I	Coupled	0.5
C6G1I	Coupled	0.1

The integration hour is 96 hours. The lateral boundary condition is changed every six hours. The momentum, sensible and latent heat fluxes are given to the ocean model. It should be noted that the normalization of DIC and ALK to a salinity of 34.1 from a salinity of 35.0 was done at the initial time of numerical simulations. In addition, ALK at the initial time are determined from the following formula.

$$ALK_{init} = \begin{cases} 2500.9T_i^{-0.0029} & T > 18.0 \\ 2299.818 & T \le 18.0 \end{cases}, \quad (1)$$

where T_i is water temperature at the i-th level of the multilayer ocean model. DIC at the initial time are determined from the formula as described in Wada et al. (2011a).

3. Results

Figure 1 compares the results of track simulations (close diamonds in A6G1I, close triangles in C6G1I, open diamonds in A6G5I and open triangles in C6G5I) with the best track (gray circles) archived in the Japan Meteorological Agency. The tracks simulated by the model agree well to the best track although the translation speed of simulated typhoons tends to be slow. A westward bias reported in Wada (2012) reduces due to a change of the width of lateral boundary relaxation sponge layers from 20 to 70.

Time series of simulated central pressures indicates that the coupled model leads to an increase in simulated central pressure after 24 h (Figure 2), corresponding to the end of the intensification except in A6G1I. Also, the central pressure in C6G5I is higher than that in C6G1I, indicating that an oceanic initial environmental field plays a crucial role in the intensity simulation of Typhoon Choi-wan.

A horizontal distribution of precipitation by SSMIS satellite microwave sensor has an asymmetric wave-number 1 pattern, implying that this typhoon changes to an occlusive cyclone (Figure 3a). The model well simulated the wave-number 1 precipitation pattern in C6G5I (Figure 3b) and C6G1I (Figure 3c). The amount of precipitation, particularly around 33° N, 143°E in C6G1I is higher than that in C6G5I. This suggests that an oceanic environmental field can affect the amount of the precipitation even around the eyewall and spiral-band region.

Time series of sea surface temperature (SST) in C6G5I (Figure 4a) and C6G1I (Figure 4b) indicate that SST decreases by nearly 2.5ºC around the KEO buoy during the integration, which is greater than that of Bond et al. (2011). The time series of pCO_2 in C6G5I (Figure 4c) and C6G1I (Figure 4d) show that pCO_2 gradually increases and then decreases after 72 h. Even though these simulations assume that pCO_2 in the atmosphere is a constant during the integration, these simulations poorly reproduce a "dramatically" increase in pCO_2 in the upper ocean. Bond et al. (2011) showed that a rapid decrease in SST (corresponding to 48 h integration time) started at 1200 UTC 19 September when the sea-level pressure suddenly decreased and ΔCO_2 rapidly increased. However, simulated SST started at 63 h, 15 h later than the result of Bond et al. (2011). The accuracy of track prediction of the typhoon, including the translation speed may be important for the variation of ΔCO_2.

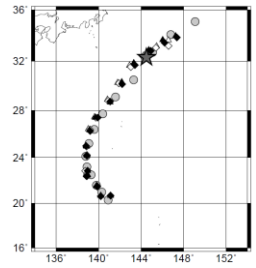

Figure 1 Best track of Choi-wan and results of track simulations from the initial time to 84h

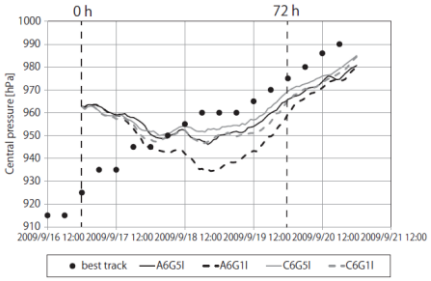

Figure 2 Best-track central pressure of Choi-wan and results of central pressure simulations from the initial time to 96h.

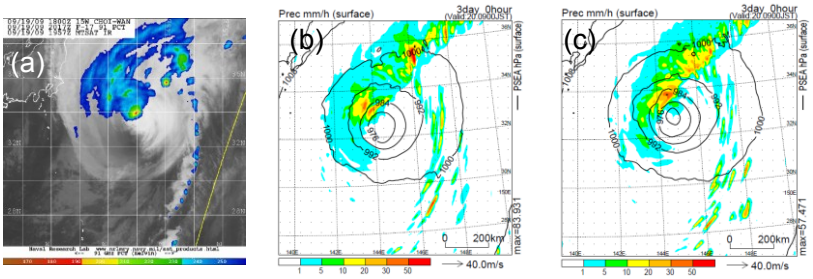

Figure 3 Horizontal distribution of precipitation (a) by SSMIS satellite microwave sensor, (b) that at 72 h in C6G5I, and (c) that at 72 h in C6G1I.

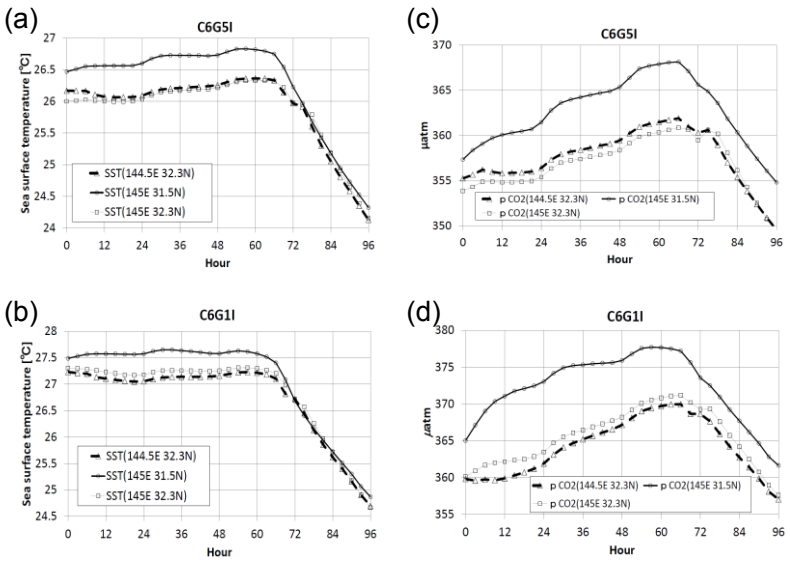

Figure 4 Time series of (a) SST in C6G5I, (b) SST in C6G1I, (c) PCO2 at the surface in C6G5I and (d) PCO2 at the surface in C6G1I around the KEO moored buoy.

4. Discussion and conclusion

This study suggests that an oceanic environmental field also affects the variation of pCO_2 in the upper ocean in addition to the effect of the translation speed of the typhoon on the variation of pCO_2 in the upper ocean. In fact, simulated SST in C6G5I is lower than that in C6G1I, resulting in low value of pCO_2 in the upper ocean.

Because of poor vertical resolution and simplified physics of the multilayer ocean model, the effect of background currents on the variation of pCO_2 in the upper ocean could not be simulated in this study. In order to investigate this issue, a sophisticated ocean general circulation model will be needed. The numerical simulations of Typhoon Choi-wan seem to be reasonable in that the track simulations agree to the best track. However, they are insufficient to reproduce the variation of SST and pCO_2 observed at the KEO buoy. We need to explore much more accuracy for the simulations.

Acknowledgement

This work was supported by the Japan Society for the Promotion of Science (JSPS), Grant-in-Aid for Scientific Research (C) (22540454) and on Innovative Areas (Research in a proposed research area) (23106505).

References

Bond, N. A., M. F. Cronin, C. Sabine, Y. Kawai, H. Ichikawa, P. Freitag, and K. Ronnholm (2011), Upper ocean response to Typhoon Choi-wan as measured by the Kuroshio Extension Observatory mooring, *J. Geophys., Res*., 116, C02031.

Usui, N., Ishizaki S., Fujii Y., Tsujino H., Yasuda T., and Kamachi M. (2006), Meteorological Research Institute multivariate ocean variational estimation (MOVE) system: Some early results. *Advances in Space Research*, **37**, 896-822.

Wada, A., 2012: *Numerical study on the effect of the ocean on tropical-cyclone intensity and structural change*, Atmospheric Models. (Ed. I. Yucel) InTech, in press.

Wada, A., T. Midorikawa, M. Ishii, and T. Motoi (2011a), Carbon system changes in the East China Sea induced by Typhoons Tina and Winnie in 1997, *J. Geophys. Res.*, **116**, C07014.

Wada, A., T. Midorikawa and M. Ishii (2011b), Variations in air-sea CO2 flux and PH induced by passage of typhoon Hai-Tang (2005), *CAS/JSC WGNE Res. Activ. Atmos. Oceanic. Modell.* **41**, 9-11

Rapid intensification of Typhoon Roke in 2011

Akiyoshi Wada*
*Meteorological Research Institute, Tsukuba, Ibaraki, 305-0052, JAPAN
awada@mri-jma.go.jp

1. Introduction

Typhoon Roke moved anticyclonically around the South Borodino Island from 16 to 19 September in 2011 and then turned to move northeastward. During the northeastward translation, Roke reached a central pressure minimum of 940 hPa. A decrease of central pressure was 30 hPa in a day just before the typhoon reached the central pressure minimum. The rapid decrease of central pressure indicates that the typhoon rapidly intensified south of Japan, around the Kuroshio region.

In 2011 typhoon season, sea surface temperature (SST) continued to be low east of the Okinawa Island from the normal value due to the subsequent passages of typhoons (for example, Ma-on, Muifa and Talas). When the typhoon passed around the low SST area, the typhoon intensified less. In addition, the typhoon rapidly intensified around the Kuroshio region where the ocean was warm. Therefore, the oceanic environment is considered to play a crucial role in the rapid intensification of Roke.

In order to understand roles of the ocean in Roke, particularly its rapid intensification, numerical simulations were performed using a nonhydrostatic atmosphere model coupled with ocean wave model and a multi-layer ocean model (Wada et al., 2010). The surface roughness length calculated by the coupled model is derived from the formulation based on wave steepness (Taylor and Yelland, 2001).

2. Experimental design

Summary of numerical simulations performed by the atmosphere-wave-ocean coupled model is listed in Table1. The coupled model covered nearly a 1600 km x 1600 km computational domain with a horizontal grid spacing of 2 km. The coupled model had 40 vertical levels with variable intervals from 40 m for the near-surface layer to 1180 m for the uppermost layer. The coupled model had maximum height approaching nearly 23 km. The integration time was 84 hours (84 h) with a time step of 6 s in the coupled model. The time step of the ocean model was six times that of the coupled model. Oceanic initial conditions were obtained from the oceanic reanalysis datasets with horizontal resolutions of 0.1º and 0.5º (Table 1) calculated by the Meteorological Research Institute multivariate ocean variational estimation (MOVE) system (Usui, et al., 2006).

Table 1 Summary of ocean coupling/noncoupling, and horizontal resolution of MOVE reanalysis of the coupled model.

Experiment	Ocean coupling	Horizontal resolution of MOVE reanalysis
A1_2km	NO	0.1º
C1_2km	YES	0.1º
A5_2km	NO	0.5º
C5_2km	YES	0.5º

3. Results

Figure 1 illustrates the results of track simulations and the best track of Roke. Simulated Roke moved north-northwestward to westward (anticyclonically) from 0 h to 36 h, whereas the best track of Roke indicates the northward translation along 131°E and then turn to northeastward from 1200 UTC 19 September (36 h integration time). According to the best track, Roke made landfall at Hamamatsu, Shizuoka Prefecture, whereas simulated typhoons made landfall in the Izu Peninsula. A difference of the track simulation caused by a difference of the initial oceanic condition is small (Fig. 1).

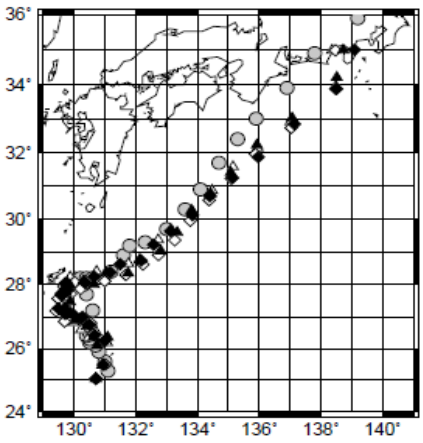

Figure 1 (Best track (gray circle) and simulated tracks in A1_2km (close diamonds), C1_2km (close triangles), A5_2km (open diamonds), and C5_2km (open triangles).

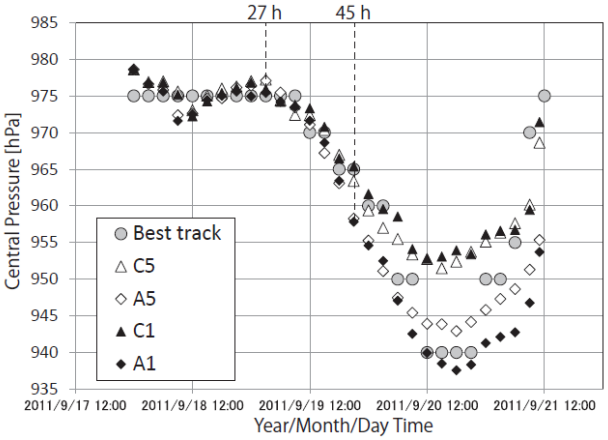

Figure 2 Time series of central pressures in A1_2km (close diamonds), C1_2km (close triangles), A5_2km (open diamonds) and C5_2km (open triangles).

Figure 2 indicates the time series of best-track central pressure and simulated central pressures. The 30 hPa rapid decrease in central pressure in a day was successfully simulated in A1_2km, whereas the rapid decrease was poorly simulated in C1_2km and C5_2km. In addition, there is a clear difference in the simulated central pressure between the oceanic reanalysis datasets of 0.1˚ and 0.5˚ horizontal resolutions. The numerical results suggest that sea surface cooling due to a passage of Roke hardly contribute the rapid intensification of Roke. In addition, oceanic environments play a crucial role in the rapid intensification.

Figures 3a-d illustrates the horizontal distribution of wind speeds at 20 m height and hourly precipitation at 27 h and 45 h, respectively. At 27 h, a low wind-speed area within a radius of maximum wind speed was clearly seen. The horizontal distribution of the wind speed was asymmetric like a wave-number 1 pattern. Hourly precipitation was high in the eastern phase of the simulated typhoon.

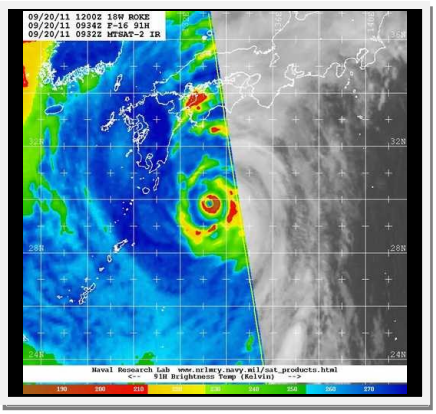

Figure 4 Horizontal distributions of 91GHz brightness temperature observed by SSMIS at 0934 UTC on 20 September (This panel is cited by http://www.nrlmry.navy.mil/tc-bin/tc_home2.cgi).

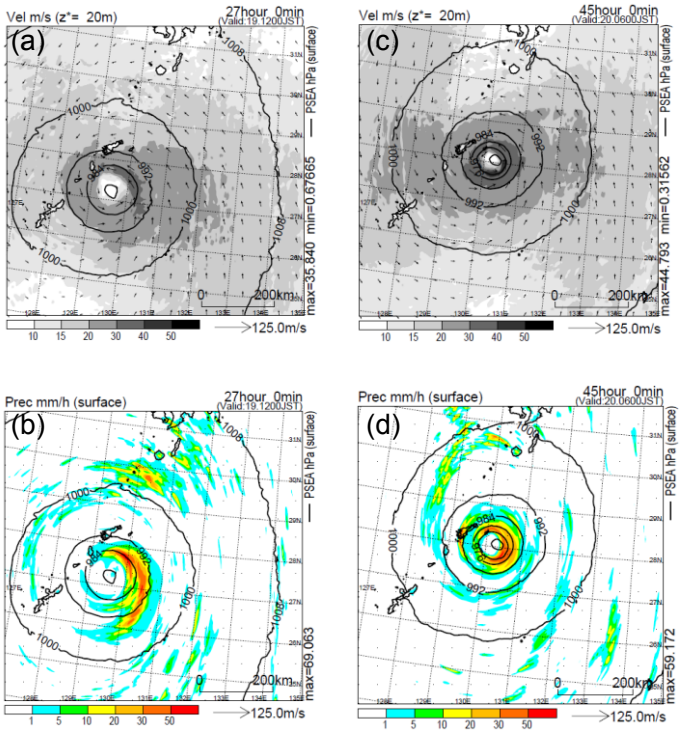

Figure 3 Horizontal distributions of (a) wind speeds at 20 m height at 27 h, (b) hourly precipitation at 27 h, (c) wind speeds at 20 m height at 45 h and (d) hourly precipitation at 45 h.

At 45 h, a low wind-speed area within a radius of maximum wind speed was narrower than that at 27 h. The horizontal distribution of the wind speed became close to the axisymmetric pattern. The maximum wind speed appeared in the southern phase of the simulated typhoon. The horizontal distribution of hourly precipitation indicates that the typhoon was shrinking during its rapid intensification. However, SSMIS microwave observation (Fig. 4) indicates secondary eyewall formation outside the primary (axisymmetric) eyewall. Moat between primary and secondary eyewalls clearly appeared in Fig. 4. This implies that finer horizontal resolution is needed to resolve the inner core dynamics of Roke. Higher horizontal resolution than 2 km is expected to develop the simulated Roke more excessively. The ocean coupling may contribute the suppression of the excessive development.

4. Discussion and conclusion

The results of the numerical simulations for Roke suggest that the horizontal resolution of 2 km is insufficient to simulate the intensity and structural change of Roke although the nonhydrostatic atmosphere model without ocean coupling well reproduce a rapid decrease of central pressure, 30 hPa in a day. We need to preform numerical simulations for Roke with a horizontal resolution less than 2 km. One of interesting themes for Roke is secondary eyewall formation and formation of concentric eyewall. In this study, an westward track error at an early integration may interrupt the secondary eyewall formation due to topography at the Amami Islands.

Acknowledgement

This work was supported by the Japan Society for the Promotion of Science (JSPS), Grant-in-Aid for Scientific Research (C) (22540454) and on Innovative Areas (Research in a proposed research area) (23106505).

References

Taylor, P. K., and M. J. Yelland (2001), The dependence of sea surface roughness on the height and steepness of the waves. *J. Phys. Oceanogr.*, **31**, 572-590.

Usui, N., S. Ishizaki, Y. Fujii, H. Tsujino, T. Yasuda, and M. Kamachi (2006), Meteorological Research Institute multivariate ocean variational estimation (MOVE) system: Some early results. *Advances in Space Research*, **37**, 896-822.

Wada, A., N. Kohno and Y. Kawai (2010), Impact of wave-ocean interaction on Typhoon Hai-Tang in 2005, *SOLA*, **6A**, 13-16.

Spin-down process caused by vortex-induced sea-surface cooling

Akiyoshi Wada
Meteorological Research Institute, Tsukuba, Ibaraki, 305-0052, JAPAN
awada@mri-jma.go.jp

1. Introduction

A vortex in the atmosphere induces sea-surface cooling (SSC), a decrease in sea-surface temperature (SST) by passage of a vortex. When the vortex is stationary, SSC appears immediately beneath the vortex. SSC plays a role in delaying vortex merger events, which are an intensification process from a several discrete mesovortices to a single ring (Wada, 2009). However, SSC little affects a structural change of the single ring at the mature phase. During the mature and decaying phases, a vortex decays as SST or the upper ocean heat content decreases immediately beneath the vortex. The decaying process of a vortex is influenced by both atmospheric and oceanic environmental conditions and their interactions. We need to understand how SSC affects the decaying process of a vortex under a unique atmospheric condition. In addition, this report addresses an issue whether or not the value of SST alone determines the intensity of the single ring. To investigate them, idealized numerical experiments were performed with reference to Wada (2009) using a nonhydrostatic model coupled with a multilayer ocean model developed at the Meteorological Research Institute in the Japan Meteorological Agency (hereafter MRIJMA).

2. Experiment design

MRINHM covered a 600 km x 600 km square computational domain with a horizontal grid spacing of 2km. MRINHM had 40 vertical levels with variable intervals from 40 m for the lowermost (near-surface) layer to 1180 m for the uppermost layer. MRINHM had maximum height approaching nearly 23 km. The time step of MRINHM was 6 s. The length of the time step of the ocean model was six times that of MRINHM. The Coriolis parameter was uniformly set to 5.0 x 10^{-5} (nearly 20ºN).

A water depth in the multilayer ocean model coupled with MRINHM was uniformly set to 1000 m. Initial SST was set to 30ºC, the initial temperature at the base of the mixed layer to 29ºC, the initial temperature at the base of the thermocline to 18ºC and the initial temperature at the bottom to 5ºC. Initial salinity was set to 35 at all levels. The initial mixed-layer depth was set to be 30 m, the initial thermocline thickness to 170 m and the initial third-layer thickness to 800 m. The third layer thickness was assumed to be unaffected by entrainment during the integration.

Table 1 summarizes the idealized numerical experiments performed using the MRINHM with and without being coupled with the ocean model. The initial vortex and thermal conditions were the same as those given by Wada (2009). The integration time was 81 h (108 h in OC54) with results output every 30 min. The sensitivity of vertical turbulent mixing in the ocean model was also evaluated using two tuning parameters: m_d=17.5 and m_d=175. The parameter m_d is associated with turbulent kinetic energy flux produced by breaking surface waves.

Table 1 Summary of key parameters of idealized MRINHM numerical experiments with and without coupling with the ocean model.

Experiment	Integration time	Beginning hour of coupled model
CTL	81 h	0 h
OC	81 h	27 h
OC54	108 h	54 h

3. Results

Figure 1 indicates that CP rapidly decreases from nearly 21 h to 42 h in OC54, indicating that the vortex rapidly intensifies when SST underneath the vortex is not changed and remains high. High value of m_d leads to high CP, indicating that rapid intensification of the vortex is suppressed in CTL and OC27, and a rapid increase in CP or a rapid weakening of strong intensity of the vortex in OC54. A difference in CP between two m_d values turns to be uniform at 81 h in all experiments. In OC54, CP monotonically decreases. Interestingly, the value of CP is nearly 985 hPa at 81 h

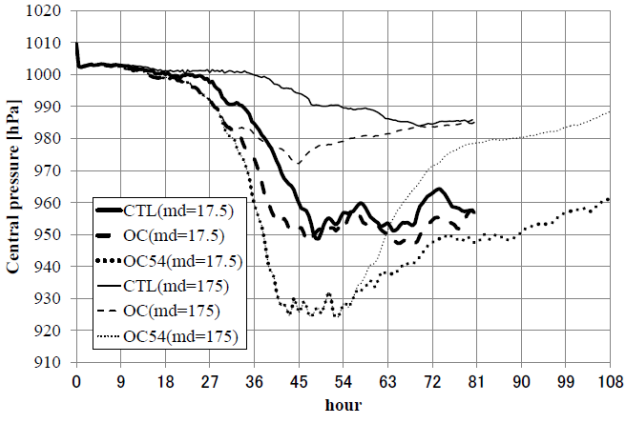

Figure 1 Time series of CP of the vortex every 30 minutes.

81h in CTL and OC, and at 108 h at OC54 when m_d = 175, whereas that is nearly 960 hPa when m_d = 17.5.

Figure 2 indicates that the variation of CP does not always correspond to that of SST when m_d = 175. The value of CP in CTL is almost the same as that in OC at 81 h and OC 54 at 108 h (nearly 22.8ºC) when m_d = 17.5. SST increases after 81 h in OC54 due to the input of solar radiation and horizontal numerical diffusion. A rapid decrease in SST (the amplitude is nearly 11ºC: Fig. 2) causes a rapid increase in CP (the amplitude is nearly 25 hPa: Fig. 1) from 54 h to 63 h in OC54 when m_d = 175, which is a characteristic of the impact of vortex-induced SSC on the vortex at the mature and decaying phases. The characteristic is different from that at the intensification phase.

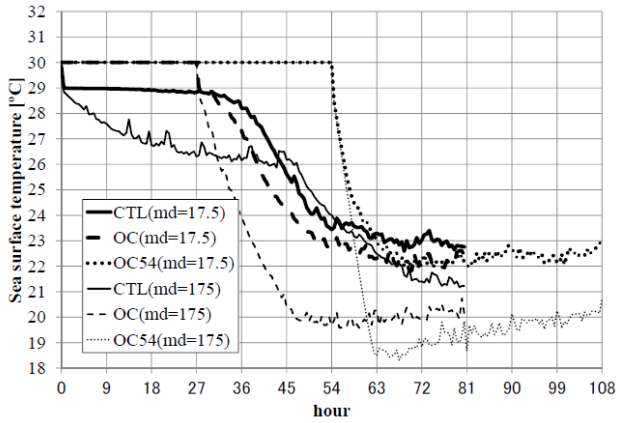

Figure 2 Time series of SST beneath a vortex every 30 minutes.

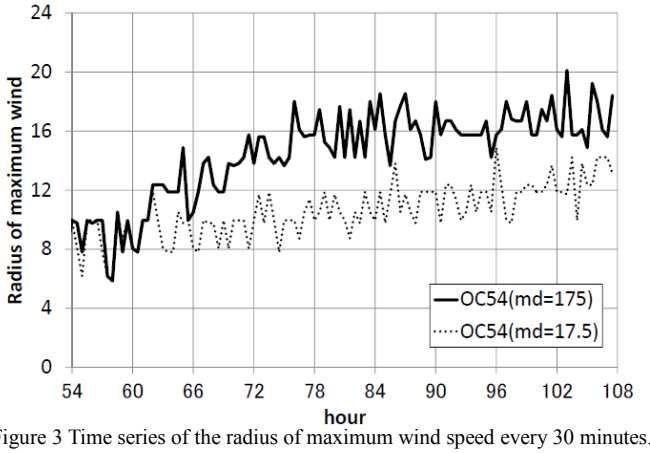

Figure 3 Time series of the radius of maximum wind speed every 30 minutes.

The radius of maximum wind speed (RMW) is nearly 8 km at 54 h (Fig. 3). RMW is extended to 12 km at 108 h in OC54 when m_d = 17.5 and is further extended to 16 km at the same hour in OC54 when m_d = 175. A difference of RMW becomes clear from 63 h to 78 h when a rapid decrease in SST terminates.

We investigate the impact of vortex-induced SSC on the gradient-wind balance of the vortex at 20-m height. Horizontal distribution of winds at 54 h (Fig. 4a) shows that the inflow around RMW is caused by anticyclonic agradient winds. Maximum winds at 81 h (Fig. 4b) are reduced to nearly 54.1 m s^{-1} from 62.0 m s^{-1}. However, the characteristics of the inflow and anticyclonic agradient winds at 81 h are not changed from those at 54h. In contrast, anticyclonic agradient winds are weak and resultant inflow becomes weak at 81 h when m_d = 175. The location of relatively strong agradient winds shift outward from the vortex's center, indicating the extension of RMW.

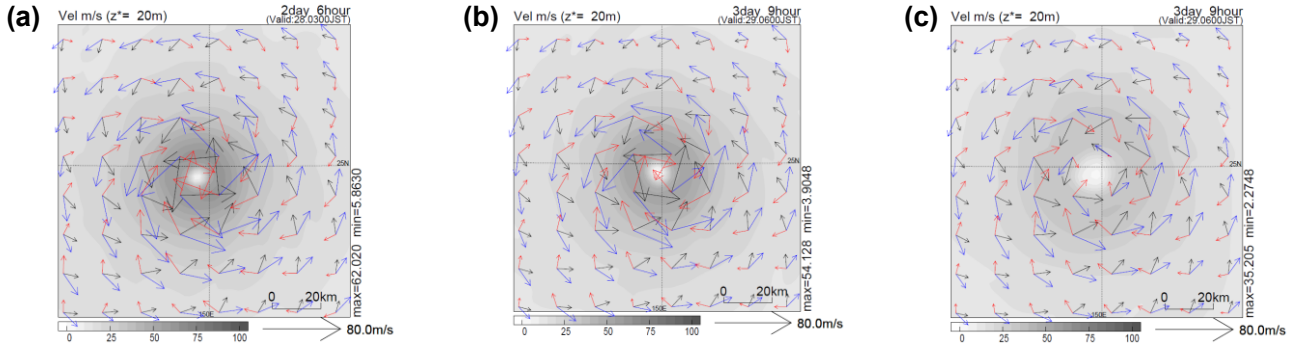

Figure 4 Horizontal distribution of winds (black), gradient winds (blue) and agradient winds (red) at 20-m height (a) at 54 h in OC54 when m_d = 17.5, (b) at 81 h when m_d = 17.5 and (c) at 81 h when m_d = 175.

4. Discussion and conclusion

A 'spin-down' process caused by vortex-induced SSC is characterized by the extension of RMW and suppression of the inflow owing to weakening agradient winds. In fact, static stability in the lower troposphere (particularly below 1000 m height) becomes relatively high in OC54 when m_d = 175 (not shown). High static stability is responsible for suppression of vertical velocity within the vortex (not shown) and resultant decrease in total water within the inner core, resulting in the weakness of pressure gradient around the location of RMW and in the reduction of horizontal winds in the lower troposphere. The reduction of winds affects both gradient and agradient winds so that both the inflow and tangential winds becomes weak. The extension of RMW is considered to be caused by weakening both inflow and angular momentum transport due to weakening surface friction.

This report describes a spin-down process caused by vortex-induced SSC. Main conclusions are:

1) CP at the mature phase is not uniquely determined by SST just beneath the vortex.
2) The impact of vortex-induced SSC on the evolution of the vortex at the mature and decaying phase differs from that at the intensification phase.
3) Vortex-induced SSC leads to an increase in static stability, resulting in the suppression of vertical velocity the reduction of total water within the inner core and the decrease in pressure gradient around RMW, and thus the extension of RMW owing to weakening both inflow and angular momentum conversation.

Acknowledgement
This work was supported by the Japan Society for the Promotion of Science (JSPS), Grant-in-Aid for Scientific Research (C) (22540454) and on Innovative Areas (Research in a proposed research area) (23106505).

References

Wada, A. (2009). Idealized numerical experiments associated with the intensity and rapid intensification of stationary tropical cyclone-like vortex and its relation to initial sea-surface temperature and vortex-induced sea-surface cooling, *Journal of Geophysical Research*, Vol. **114**, D18111.

Oceanic influences for a large eye of Typhoon Talas in 2011

Akiyoshi Wada*
*Meteorological Research Institute, Tsukuba, Ibaraki, 305-0052, JAPAN
awada@mri-jma.go.jp

1. Introduction

Tropical cyclones with a large eye are often called as 'annular' tropical cyclones, a symmetric category of tropical cyclones (Knaff et al., 2003). According to Weatherford (1984), eyes with diameters > 85 km are considered to be large. The radius of 15 kt wind speed of Typhoon Talas was from 500 to 650 km when its minimum central pressure was 970 hPa. Talas made landfall in Japan at around 1000 JST on 3 September and caused torrential rainfalls particularly the Kii peninsula. One of peculiar features of Talas was the maintenance of a large eye when Talas moved northward and turned to northwestward until the typhoon made landfall in Japan. The translation speed of Talas was estimated to be nearly 1.3 m s^{-1} from 26 to 30 August, which was slower than the phase speed of the first baroclinic mode in the ocean. The slow translation speed of Talas is considered to be favorable for lowering sea surface temperature beneath the typhoon.

In order to understand oceanic influences on Talas, particularly its large eye, numerical simulations were performed using a nonhydrostatic atmosphere model coupled with an ocean wave model and a multi-layer ocean model (Wada et al., 2010). The surface roughness length calculated by the coupled model is derived from the formulation based on wave steepness (Taylor and Yelland, 2001).

2. Experimental design

Summary of numerical simulations performed by the atmosphere-wave-ocean coupled model is listed in Table 1. The coupled model covered nearly a 3600 km x 5000 km computational domain with a horizontal grid spacing of 6 km. The coupled model had 40 vertical levels with variable intervals from 40 m for the near-surface layer to 1180 m for the uppermost layer. The coupled model had maximum height approaching nearly 23 km. The integration time was 120 hours (120 h) with a time step of 15 s in the coupled model. The time step of the ocean model is six times that of the coupled model.

Table 1 Summary of ocean coupling/noncoupling, parameters of Rayleigh damping associated with the lateral boundary condition (PRD), and horizontal resolution of MOVE reanalysis of the coupled model.

Experiment	Ocean coupling	PRD	Horizontal resolution of MOVE reanalysis
A1_IDIFX15	NO	15	0.1º
C1_IDIFX15	YES	15	0.1º
A5_IDIFX15	NO	15	0.5º
C5_IDIFX15	YES	15	0.5º
C5_IDIFX5	YES	5	0.5º
C5_IDIF150	YES	150	0.5º

The sensitivity of parameters (the value of horizontal grids is 5, 15, 150, respectively) of Rayleigh damping associated with the lateral boundary condition to the simulated track of Talas was investigated in order to examine the influence of environmental atmospheric conditions on the track of Talas.

Oceanic initial conditions were obtained from the oceanic reanalysis datasets with horizontal resolutions of 0.1º and 0.5º calculated by the Meteorological Research Institute multivariate ocean variational estimation (MOVE) system (Usui, et al., 2006). Because the southern limit of the domain in the MOVE system with a horizontal resolution of 0.1º was 15ºN, the oceanic reanalysis data with a horizontal resolution of 0.5º were merged south of 15ºN when the oceanic reanalysis data with a horizontal resolution of 0.1º was used as an oceanic initial condition.

3. Results

Figures 1a-b show the results of track simulations and the best track of Talas. Simulated Talas moved north along 139°E from 12 h to 54 h in A5_IDIFX15 (Table 1), whereas the best track of Talas indicates the northward translation along 140°E and then turn to northwestward from 0600 UTC 30 August (at 90 h). The parameters of Rayleigh damping associated with the lateral boundary condition clearly affected the track of Talas: When the value was high, simulated Talas tended to move westward, while the typhoon tended to move northward when the value was low (Fig. 1a).

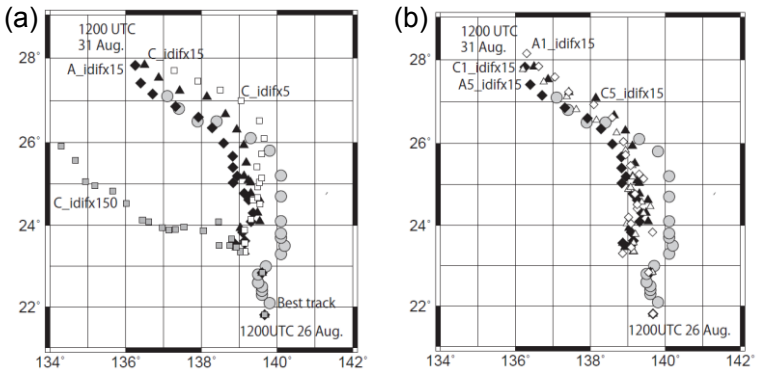

Figure 1 (a) Best track and simulated tracks in A5_IDIFX15 (close diamonds), C5_IDIFX15(close triangles), C5_IDIFX5(open squares), and C5_IDIFX150(gray squares). (b) Same as Fig.1(a) except in A5_IDIFX15, C5_IDIFX15, A1_IDIFX15 (open diamonds), and C1_IDIFX15 (open triangles).

A difference of initial oceanic condition led to a difference of the time when the simulated Talas was recurved: When the oceanic reanalysis data with a horizontal resolution of 0.5° were used, the recurvature occurred earlier (54 h in A5_IDIFX15 and 60 h in C5_IDIFX15) than that (72 h in A1_IDIFX15 and 78 h in C1_IDIFX15)when the data with a horizontal resolution of 0.5° were used (Fig.1b).

Figure 2 show the time series of simulated central pressures and best-track central pressure when the parameter of Rayleigh damping associated with the lateral boundary condition was set to 15. Simulated central pressures in A1_IDIFX15 and A5_IDIFX15 underwent rapid intensification from 24 h to 60 h, corresponding to the northward translation of Talas. A central pressure minimum in A1_IDIFX15 was 938.2 hPa in A1_IDIFX15 (at 96 h) and 942.6 hPa in A5_IDIFX (at 120 h), while a central pressure minimum was 968.9 hPa in C5_IDIFX15 (at 60 h) and 966.5 hPa in C1_IDIFX15 (at 72 h). The central pressure minima in C1_IDIFX15 and C5_IDIFX15 were closer to the best-track central pressure minimum (970hPa) than those in A5_IDIFX15 and A1_IDIFX15.

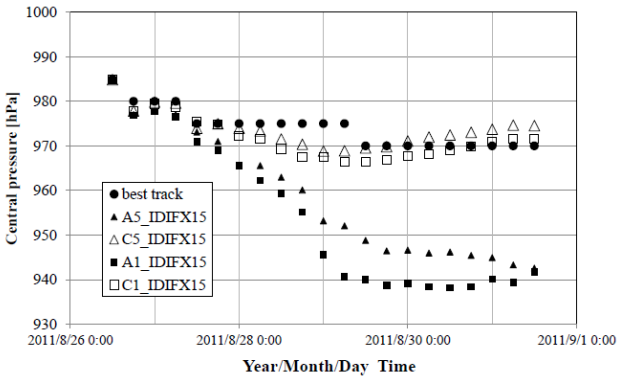

Figure 2 Time series of central pressures in A5_IDIFX15, C5_IDIFX15, A1_IDIFX15 and C1_IDIFX15.

As described in the introduction, a large eye of Talas is one of peculiar features in that a large eye had no debris or mesovortex inside the eyewall, differently from previous annular hurricanes (Knaff et al., 2003) and Typhoon Winnie in 1997 (Zhang et al., 2005). Figure 3 indicates the time series of the radius of maximum wind speed at the lowermost level (corresponding to the height of 20 m). After 48 h, the radius seems to be stationary and become large monotonically. The average of the radius from 48 h to 120 h was 94.7 km in A5_IDIFX, 92.0 km in A1_IDIFX, 108.3 km in C5_IDIFX and 103.5 km in C1_IDIFX, indicating that the ocean coupling results in the enlargement of the radius of maximum wind speed of Talas.

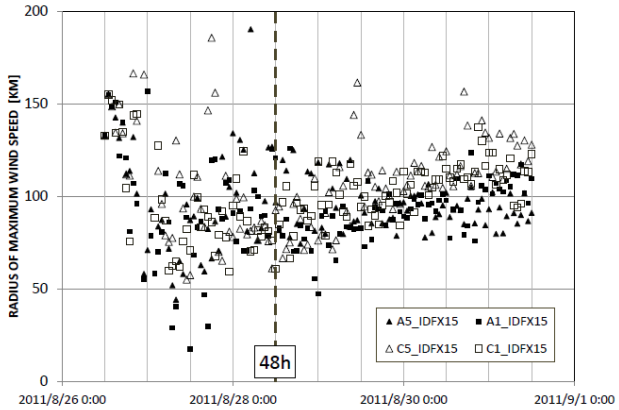

Figure 3 Same as Fig. 2 except for the radius of maximum wind speed at the lowermost level of the coupled model.

4. Discussion and conclusion

The results of the numerical simulations suggest that the upper ocean response (including sea-surface cooling beneath the typhoon) to Talas contributes to the enlargement of the radius of maximum wind speed of Talas to some extent in addition to the suppression of its excessive intensification. The sensitivity experiments associated with the parameters of Rayleigh damping suggests that excessively high value interrupts the precise track simulation of Talas. However, Talas was indeed formed in the eastern part of the subtropical cyclonic gyre and the gyre included Typhoon Nanmadol in the western part of the gyre. How the gyre affected Talas directly or indirectly as an atmospheric environmental factor should be explored because it is considered to be related to how much the value of Rayleigh damping parameter should be set.

For Talas, the horizontal resolution of 6 km is sufficient to reproduce the (maximum) intensity of Talas. For a typhoon with a large eye, ocean coupling might be indispensable for reproducing the intensity realistically.

Acknowledgement

This work was supported by the Japan Society for the Promotion of Science (JSPS), Grant-in-Aid for Scientific Research (C) (22540454) and on Innovative Areas (Research in a proposed research area) (23106505).

References

Knaff, J. A., J. P. Kossin, and M. DeMaria (2003), Annular hurricanes. *Wea. Forecasting*, **18**, 204-223.

Taylor, P. K., and M. J. Yelland (2001), The dependence of sea surface roughness on the height and steepness of the waves. *J. Phys. Oceanogr.*, **31**, 572-590.

Usui, N., S. Ishizaki, Y. Fujii, H. Tsujino, T. Yasuda, and M. Kamachi (2006), Meteorological Research Institute multivariate ocean variational estimation (MOVE) system: Some early results. *Advances in Space Research*, **37**, 896-822.

Wada, A., N. Kohno and Y. Kawai (2010), Impact of wave-ocean interaction on Typhoon Hai-Tang in 2005, *SOLA*, **6A**, 13-16.

Weatherfold, C. L. (1984), Typhoon structural variability. Colorado State University, Atmospheric Science Paper 391, 77pp.

Zhang, Q.-H., Chen, S.-J., Kuo, Y.-H., Lau, K.-H., and R. A. Anthes (2005), Numerical study of a typhoon with a large eye: Model simulation and verification. *Mon. Wea. Rev.*, **133**, 725-742.

Impact of surface roughness lengths on simulations of Typhoon Fanapi (2010)

Akiyoshi Wada* and Nadao Kohno**

*Meteorological Research Institute, Tsukuba, Ibaraki, 305-0052, JAPAN
**Japan Meteorological Agency, Chiyoda, Tokyo, 100-8192, JAPAN
*awada@mri-jma.go.jp

1. Introduction

Surface roughness lengths over the ocean are varied by ocean waves. The surface roughness length is used in the atmosphere model to determine exchange coefficients for momentum, sensible and latent heat fluxes. The sensible and latent heat fluxes play a crucial role in developing a tropical cyclone, while the momentum flux drives the upper ocean, resulting in sea-surface cooling by passage of a tropical cyclone. The exchange coefficient for the momentum flux is also important to estimate the effect of surface friction near the surface on angular momentum transport, which plays a role in reducing tangential winds and producing radial inflow and thus secondary circulation.

In order to understand the effect of surface roughness lengths on simulations of tropical cyclones, the impact of surface roughness lengths on simulations of tropical cyclones is investigated for Typhoon Fanapi (2010) using a nonhydrostatic atmosphere model coupled with an ocean wave model and a multi-layer ocean model (Wada et al., 2010). The surface roughness length calculated by the coupled model is determined by the following five methods, respectively; functions of wave-induced stress (Janssen, 1991), wave age (Smith, 1992), wave steepness (Taylor and Yelland, 2001), the assumption of Charnock constant (Charnock, 1955), and drag coefficients depending on 10-m wind speed (Kondo, 1975).

2. Experimental design

Ten numerical simulations were performed for Fanapi, which was one of targeted typhoons in the Impacts of Typhoons on the Ocean in the Pacific (ITOP) program ITOP, by the coupled model incorporating the above-mentioned surface roughness length scheme (Table 1). The coupled model covers a 2000 km x 1800 km computational domain with a horizontal grid spacing of 2 km. The coupled model has 40 vertical levels with variable intervals from 40 m for the near-surface layer to 1180 m for the uppermost layer. The coupled model has maximum height approaching nearly 23 km. The integration time is 72 hours with a time step of 6 s in the atmosphere model.

Table 1 List of numerical simulations, surface roughness scheme used, and horizontal resolution of oceanic initial condition.

Experiment		Surface roughness scheme	Horizontal resolution of MOVE
CH	CH1	Charnock (1955)	0.1°
	CH5		0.5°
JA	JA1	Janssen (1991)	0.1°
	JA5		0.5°
KO	KO1	Kondo (1975)	0.1°
	KO5		0.5°
SM	SM1	Smith (1992)	0.1°
	SM5		0.5°
TY	TY1	Taylor and Yelland (2001)	0.1°
	TY5		0.5°

Oceanic initial conditions were obraied from the oceanic reanalysis datasets with horizontal resolutions of 0.1º and 0.5º, calculated by the Meteorological Research Institute multivariate ocean variational estimation (MOVE) system (Usui, et al., 2006). Because the southern limit of the domain in the MOVE system with a horizontal resolution of 0.1º was 15ºN, the oceanic reanalysis data with a horizontal resolution of 0.5º were merged south of 15ºN when the dataset with a horizontal resolution of 0.1º was used as an oceanic initial condition.

After surface roughness lengths are calculated by each above-mentioned method, wind speeds at 10-m height and drag coefficients are calculated by the method proposed by Louis et al., (1982). Except the method of Taylor and Yelland (2001), an iteration method is applied for determining surface roughness length and frictional velocity. The dependency of wave steepness on a wind direction is applied only in the method of Taylor and Yelland (2001): When the wind direction is perpendicular to the wave direction, this study assumes that wave steepness does not grow up and reduces by half.

3. Results

The numerical result indicates that the simulated track of Fanapi had a northward bias, which was independent of the choice of surface roughness length scheme (Fig.1a). In addition, the result of track simulation is not affected by the horizontal resolution of oceanic initial data (not shown).

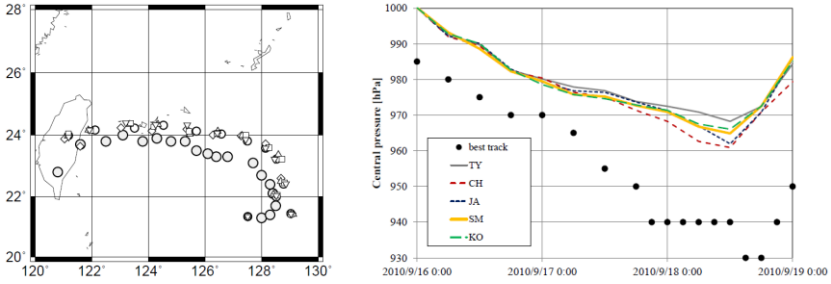

Figure 1 (a) Best track of Fanapi (Large gray circles) and simulated tracks (TY: small open circles, CH: open diamonds, JA: open triangles, SM: open squares, and KO: open inverse triangles). (b) time series of best-track central pressure and simulated ones.

The horizontal resolution is also irrelevant to the central-pressure simulations (not shown). However, the central-pressure simulations depend on a surface roughness length scheme even though all simulated central pressures are higher than the best-track central pressure. A difference in the average of simulated central pressure among five schemes is nearly 10 hPa at 60 h (Fig.1b). The difference becomes markedly when the simulated Fanapi undergoes intensification.

Figure 2 indicates that drag coefficients are high at 60 h under relatively low winds. Edson et al. (2007) reported that drag coefficients were relatively high under extremely low winds. The drag coefficient may be overestimated compared to the result of Edson et al. (2007). The dependency of 10-m wind speed on drag coefficient indicates that drag coefficients monotonically increase with an increase in 10-m wind speeds except that derived from Taylor and Yelland (2001) (Fig.2). The dependency derived from Taylor and Yelland (2001) indicates that drag coefficients clearly level off and are saturated when 10-m wind speed is higher than 30 m s^{-1}. This dependency is also seen in the dependency of surface roughness lengths on 10-m wind speeds (Fig. 3).

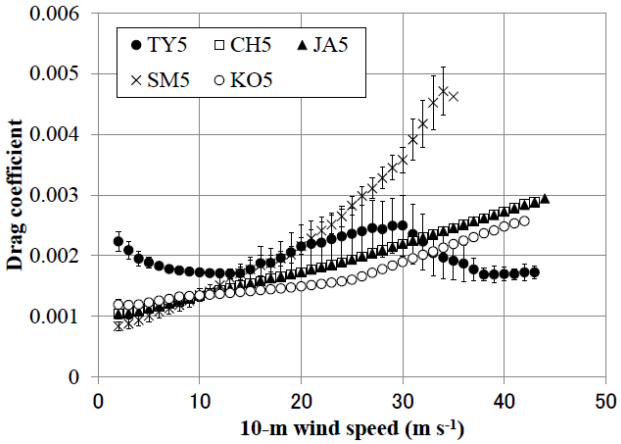

Figure 2 The relation of 10-m wind speed to drag coefficients obtained from numerical simulations listed in Table 1.

In contrast, drag coefficients increases linearly when the wave age, the ratio of the phase speed to frictional velocity, is used for determining surface roughness lengths, which are calculated by the formula of Smith et al. (1992), except at 35 m s^{-1}. The values of drag coefficients and surface roughness lengths are much higher than those by any other formulae. However, there is little impact of high values of drag coefficient and surface roughness length on simulations of the track of Fanapi and a small impact on its intensity at the mature phase.

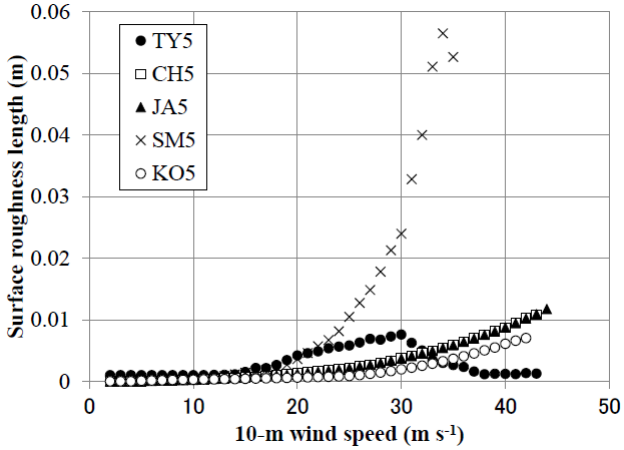

Figure 3 The relation of 10-m wind speed to surface roughness lengths obtained from numerical simulations in Table 1.

Not only Smith et al., (1992) but also other methods except Taylor and Yelland (2001) had a strong dependency of drag coefficients and surface roughness lengths on frictional velocity. This is why surface roughness lengths must be solved by iteration algorithm. Wave steepness, however, is determined from a wave-length scale and wave height, not directly dependent of frictional velocity.

4. Discussion and conclusion

From numerical simulations for Fanapi, drag coefficients derived from the formula of Taylor and Yelland (2001) alone markedly level off when 10-m wind speeds are over 30 m s^{-1}. There is little impact of surface roughness lengths on the track of Fanapi and a small impact on its intensity at the mature phase, but there may be impacts on the structure such as the radius of maximum wind speed and precipitation pattern. In addition, we need to investigate the impacts not only at the intensification phase but also the mature and decaying phases.

Acknowledgement

This work was supported by the Japan Society for the Promotion of Science (JSPS), Grant-in-Aid for Scientific Research (C) (22540454) and on Innovative Areas (Research in a proposed research area) (23106505).

References

Charnock, H. (1955), Wind stress on a water surface, *Quart. J. Roy. Meteor. Soc.*, **81**, 639-640.

Jansen, P. A. E. M. (1991), Quasi-linear theory of wind-wave generation applied to wave forecasting, *J. Phys. Oceanogr.*, **21**, 1631-1642.

Edson, J., T. Crawford, J. Crescenti, T. Farrar, N. Frew, G, Gerbi and Coauthors (2007), The Coupled Boundary Layers and Air–Sea Transfer Experiment in Low Winds. *Bull. Amer. Meteor. Soc.*, **88**, 341–356.

Kondo, J. (1975), Air-sea bulk transfer coefficients in diabatic conditions. *Bound. Layer Meteor.*, **9**, 91-112.

Louis, J. F., M. Tiedtke, and J. F. Geleyn (1982), A short history of the operational PBL parameterization at ECMWF. Proc. *Workshop on Planetary Boundary Layer Parameterization, Reading, United Kingdom*, ECMWF, 59–79.

Smith, S. D., R. J. Anderson, W. A. Oost, C. Kraan, N. Maat, J. Decosmo, K. B. Katsaros, K. L. Davidson, K. Bumke, L. Hasse, and H. M. Chadwick (1992), The HEXOS results. *Boundary-Layer Meteorol.*, **60**, 109-142.

Taylor, P. K., and M. J. Yelland (2001), The dependence of sea surface roughness on the height and steepness of the waves. *J. Phys. Oceanogr.*, **31**, 572-590.

Usui, N., S. Ishizaki, Y. Fujii, H. Tsujino, T. Yasuda, and M. Kamachi (2006), Meteorological Research Institute multivariate ocean variational estimation (MOVE) system: Some early results. *Advances in Space Research*, **37**, 896-822.

Wada, A., N. Kohno and Y. Kawai (2010), Impact of wave-ocean interaction on Typhoon Hai-Tang in 2005, *SOLA*, **6A**, 13-16.